Near Surface Geophysics, 2015, **13**, 61-72 doi:10.3997/1873-0604.2014041

Joining multiple AEM datasets to improve accuracy, cross calibration and derived products: The Spiritwood VTEM and AeroTEM case study

Vincenzo Sapia[1*], Andrea Viezzoli[2] and Greg Oldenborger[3]

[1] *Istituto Nazionale di Geofisica e Vulcanologia, Via di Vigna Murata 605, 00143, Rome, Italy*
[2] *Aarhus Geophysics Aps, C.F. Møllers Alle 4, Aarhus C 8000, Denmark*
[3] *Geological Survey of Canada, Natural Resources Canada, 601 Booth Street, Ottawa, ON, Canada*

Received January 2014, revision accepted July 2014

ABSTRACT

Airborne time-domain electromagnetic methods (AEM) are useful for hydrogeological mapping due to their rapid and extensive spatial coverage and high correlation between measured magnetic fields, electrical conductivity, and relevant hydrogeological parameters. However, AEM data, pre-processing and modelling procedures can suffer from inaccuracies that may dramatically affect the final interpretation. We demonstrate the importance and the benefits of advanced data processing for two AEM datasets (AeroTEM III and VTEM) collected over the Spiritwood buried valley aquifer in southern Manitoba, Canada. Early-time data gates are identified as having significant flight-dependent signal bias that reflects survey flights and flight lines. These data are removed from inversions along with late time data gates contaminated by apparently random noise. In conjunction with supporting information, the less-extensive, but broader-band VTEM data are used to construct an electrical reference model. The reference model is subsequently used to calibrate the AeroTEM dataset via forward modelling for coincident soundings. The procedure produces calibration factors that we apply to AeroTEM data over the entire survey domain. Inversion of the calibrated data results in improved data fits, particularly at early times, but some flight-line artefacts remain. Residual striping between adjacent flights is corrected by including a mean empirical amplitude correction factor within the spatially constrained inversion scheme. Finally, the AeroTEM and VTEM data are combined in a joint inversion. Results confirm consistency between the two different AEM datasets and the recovered models. On the contrary, joint inversion of unprocessed or uncalibrated AEM datasets results in erroneous resistivity models which, in turn, can result in an inappropriate hydrogeological interpretation of the study area.

INTRODUCTION

Several countries have acquired, over the past decades, airborne electromagnetic (AEM) data covering large areas. The original applications were most often used for promoting mineral exploration (Palacky and West 1991) or for hydrogeological mapping (Auken *et al*. 2003, Siemon *et al*. 2009, Steuer *et al*. 2009, Jørgensen *et al*. 2012). In Canada, many electromagnetic surveys are proprietary and a few are public domain and duly compiled in accessible databases. The type and quality of the data also varies significantly, from older datasets from the 1990s or earlier, to more modern ones. The significant developments in data processing and modelling of the last few years, accompanied by novel approaches to integration of multiple datasets of different types, are driving research in revisiting these existing datasets (e.g., Sorensen, Munday and Cahill 2012). One approach to reconciling multiple data sets from different systems, or different generations of data is through calibration of lower quality data with a better quality dataset, and subsequent joint inversion.

Lines *et al*. (1988) define the objective of joint inversion as obtaining a model which is consistent with all available geophysical data. Examples of joint inversion of different data types for a common model of electrical conductivity exist for magnetotelluric and vertical electrical sounding data (Vozoff and Jupp 1975), time-domain electromagnetic and magnetotelluric data (Meju 1996), and time-domain electromagnetic and electrical data (Raiche *et al*. 1985, Schmutz *et al*. 2000, Christiansen *et al*. 2007, Santos *et al*. 2010). In this paper, we consider calibration and joint spatially constrained inversion of two AEM datasets collected over the same survey area using different systems at different times. In this case, the data type, the physics and the earth model are the

* vincenzo.sapia@ingv.it

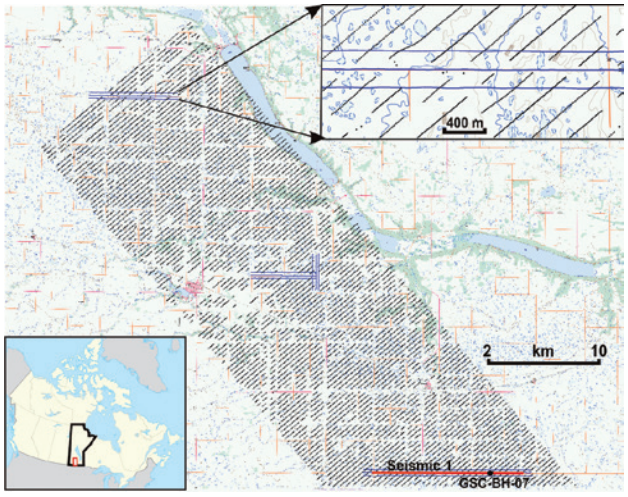

FIGURE 1
Location of the Spiritwood valley survey area in southern Manitoba, Canada. The blue dots correspond to VTEM survey soundings and the black dots to the AeroTEM survey soundings (where culturally-affected soundings have been removed). The solid red line indicates the location of a seismic reflection section and the black dot indicates the location of borehole GSC-SW-07. The top inset shows an area of survey overlap. AeroTEM line spacing is 400 m (oblique lines) and VTEM line spacing is 300 m (horizontal lines).

same such that the inversion is truly joint as opposed to sequential (Lines 1988) or structural in nature (e.g., Wisén and Christiansen 2005). We suggest that in the presence of multiple datasets, due processing, inversion, post-processing, data correction (calibration) and joint inversion is the proper approach, capable of providing reliable and consistent resistivity models to be interpreted for geological and/ or hydrogeological purposes.

METHODOLOGY

We start with processing and inversion of an AeroTEM III helicopter time-domain electromagnetic (HTEM) dataset commissioned by the Geological Survey of Canada in 2010 as part of an aquifer mapping campaign for the Spiritwood valley in Manitoba, Canada (Fig. 1, Oldenborger *et al*. 2013). Deliverables from contractors often include raw data and Conductivity Depth Images (CDIs, Macnae *et al*. 1991, Huang and Rudd 2008). These are imaging products based on approximations, and not inversions based on accurate forward modelling. As such, they may be inadequate for providing accurate rendering of the subsurface resistivity variations required for rigorous hydrogeological mapping. In addition, the data used to produce CDIs are often not processed to account for system bias, noise levels, or coupling with cultural infrastructure. We therefore begin with a complete reprocessing of the raw TEM data. The raw TEM data are first assessed to identify regions of cultural interference often associated with roads and power lines (Danielsen *et al*. 2003). Affected soundings are removed and remaining soundings are averaged to a spatial interval of approximately 25 m at the ground surface but with increasing width at depth (Auken *et al*. 2009). After averaging, the noise level at all times was assessed and estimates were assigned to individual soundings.

The averaged data are used as input to a Spatially Constrained Inversion (SCI, Viezzoli *et al*. 2008). Within the SCI, the forward model incorporates a unique transmitter-receiver synchronization for each survey flight based on the transmitter waveform recorded during calibration. This results in effective gate times that are different from the nominal time gates reported by the contractor, a difference that is more important at earlier gates. The peak current of the transmitter waveform was varied according to that monitored for each transient. The transmitter height above ground surface was calculated as the difference of helicopter navigation data and nominal offset of the transmitter frame. Such offset cannot be considered constant, and height is therefore included as an inversion parameter.

For calibration purposes, we employ a "full waveform" VTEM dataset collected by Geotech Ltd. over a small portion of the AeroTEM survey area (Fig. 1, Legault *et al*. 2012). The AeroTEM calibration procedure is adapted from that applied in Denmark to AEM data whereby an electrical reference model is derived from ground TEM data (Foged *et al*. 2013). In this case, the reference models are derived from inversions of the VTEM data that are verified against ERT, seismic and borehole data (Sapia *et al*. 2014). For positions of overlapping soundings, the AeroTEM response is modelled on the VTEM-derived reference model and the result is compared to the observed AeroTEM data. A time shift of the data gates is applied to force general equality (within noise levels) between the modelled and observed AeroTEM responses. Given the small nature of the time shift, it is predominantly the early-time data that are affected by this calibration. In theory, the procedure could also include an amplitude shift for all gates.

As a final step, we perform a joint inversion of both the AeroTEM and VTEM data. Using the SCI framework, constraints in model space can be applied across inversion of the VTEM and AeroTEM data in areas of overlap. This exercise allows for a check on the level of system consistency and cross calibration achieved between the two AEM datasets.

RESULTS

AeroTEM III

Figure 2 shows the electrical resistivity model recovered from inversion of the raw AeroTEM voltage data as received from the contractor. The model has 29 layers with layer thickness logarithmically increased up to a depth of 200 m. The data have not been edited for cultural interference, system bias, or excessive late-time noise; all time gates are employed, but flight-by-flight synchronization has been applied. To visualize the resistivity structures of the survey area a number of maps of resistivity averaged over different depth intervals are presented. A large amount of striping is apparent along with significant contrasts in recov-

ered resistivity between areas that systematically correspond to different flight blocks. These flight-related artefacts persist to depths in excess of 100 m where they are joined by additional artefacts resulting from culture-related noise that has not been removed from the data.

In addition to the readily apparent artefacts, the initial inversion results conflict with supporting geological knowledge of the survey area that suggests a resistive surface (e.g., Crow *et al*. 2012). Except for a limited area with a resistive surface response, we observe a conductive response for the shallowest layers over the entire survey block (Fig. 2a). Deeper resistivity maps (Figs 2b and c) hint to the existence of several resistive valley-like features at different scales. The resistive features depict a regional structure, interpreted to be the Spiritwood buried valley system, set within a conductive background, interpreted as shale bedrock (Pugin *et al*. 2014). From these inversions, we conclude that there is appreciable geological information content in the data, but that the signal at early time is too high. We posit that this early time bias is likely due to self-response of the system (residual primary field) that varies for each survey flight (Macnae and Baron-Hay 2010, Sapia *et al*. 2014). The result is that the forward response cannot fit the first two gates of data within the noise level. Without being able to conclusively identify or model system bias, a number of the early time gates must be removed from the inversion process. In this case, the first 2 or 3 gates are omitted from all subsequent inversions such that the first usable gate corresponds to approximately 120 μs after the end of the waveform ramp-off. The variability of the number of gates omitted may be attributed to geological variation across the area, the difference in the flight-by-flight magnitude of the self-response, or the difference in the degree of line-by-line levelling carried out by the contractor.

Figure 3 shows the electrical resistivity model recovered after biased early-time gates were removed and culturally-affected soundings were culled. In general, the updated resistivity maps more clearly show the existence of the Spiritwood valley as an elongate, resistive feature approximately 10 km wide. Along the middle of the regional valley we observe a narrower structure interpreted to be an inset valley, approximately 1 km wide, that follows the main valley. The resistive signature of this valley may be indicative of coarse grained sediments (i.e., sand and gravels) with aquifer potential. In addition to the inset valley, multiple resistive valley-like features are observed outside of the regional Spiritwood valley (see also Oldenborger *et al*. 2013; Pugin *et al*. 2014). Some of the resistive features are very narrow and reveal a complex glacial setting similar to observations of tunnel valleys in Denmark (Jørgensen and Sandersen 2006).

Comparison to Supporting Data

Seismic data (Pugin *et al*. 2009) and limited borehole data (Crow *et al.* 2012) allow for direct comparison with the AEM resistivity model where surveys overlap. A seismic reflection section along the southern border of the survey area is shown in Fig. 4. The main incised valleys are observed in the seismic data as a low-to-high amplitude discontinuous reflection facies and the interpreted bedrock surface (black line, Fig. 4b) is derived from the transition to low-amplitude reflections with limited penetration (Pugin *et al*. 2014). The overlying till package is manifest as high-amplitude, continuous reflections with the shallowest reflector (red line, Fig. 4b) interpreted to be an interface between

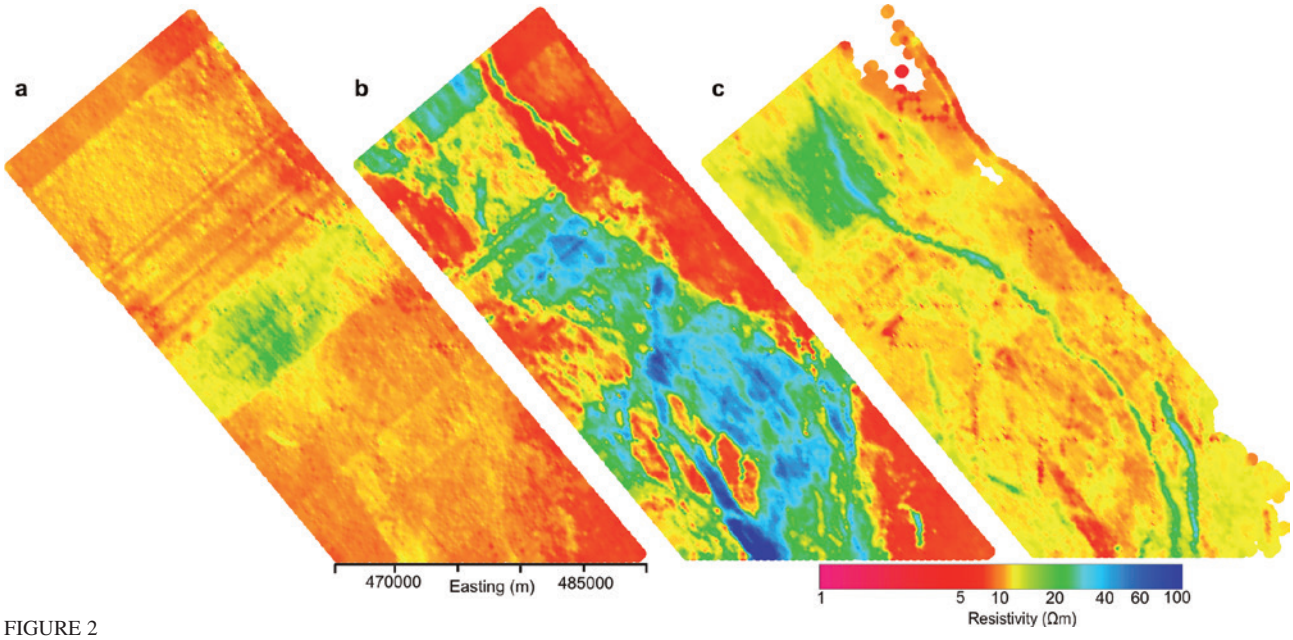

FIGURE 2

Inversion results for unprocessed AeroTEM III data. The recovered resistivity model is shown as maps of resistivity averaged over different depth intervals: a) 0–10 m, b) 50–60 m and c) 110–120 m.

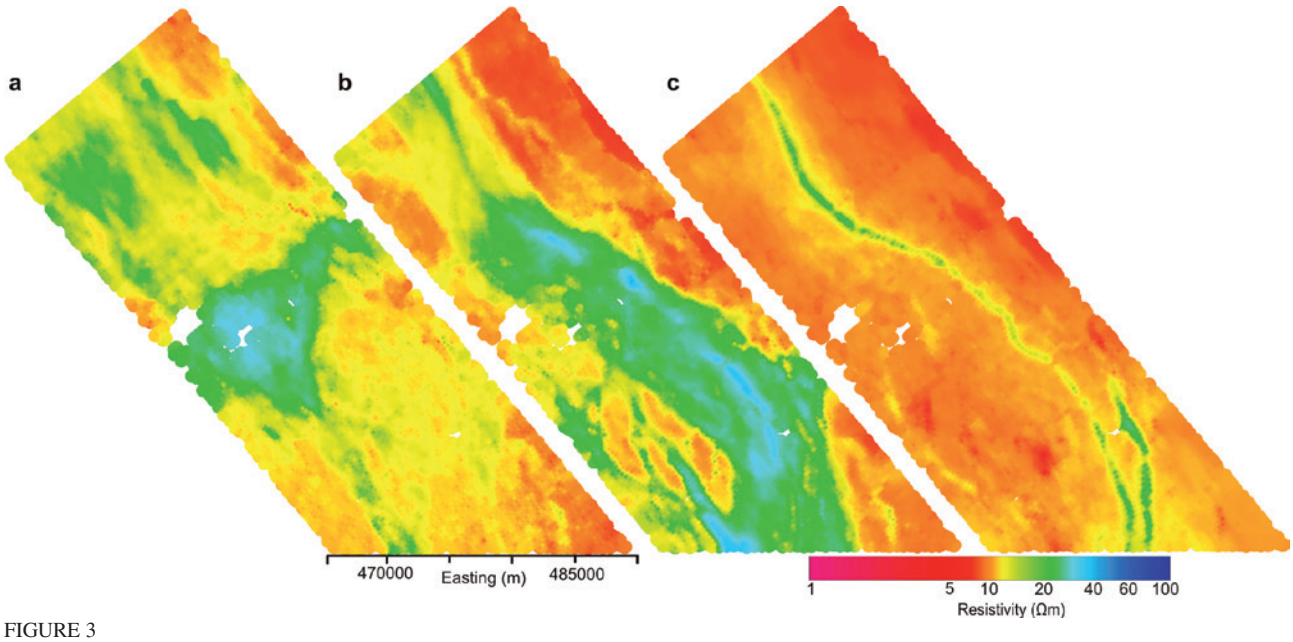

FIGURE 3

Inversion results for fully-processed AeroTEM III data. Culturally-affected soundings, biased early-time gates and excessively noisy late-time data have been removed. The recovered resistivity model is shown as maps of resistivity averaged over different depth intervals: a) 0–10 m, b) 50–60 m and c) 110–120 m. Resistivity is interpolated between soundings for mapping purposes with a search radius of 500 m such that locations of removed soundings are not readily apparent.

hard, compact till below and heterogeneous less-compact sandy till above (Pugin *et al*. 2011, Oldenborger *et al*. 2013). These reflection surfaces are interpolated and plotted on the SCI resistivity model in order to directly compare both outcomes (Fig 4a).

The top of the bedrock is readily apparent in the AEM resistivity model as a conductive boundary overlain by resistive materials (Fig. 4a). In general, the AEM result shows good agreement with the seismic information in terms of depth to bedrock, although the AEM results seem to slightly overestimate it. In some cases, there is no indication of a valley bottom in the resistivity model despite a corresponding strong change in reflection facies (Fig. 4a, from 6.3 to 9 km). The conductive bedrock at the bottom of the buried valley may be deeper than the system's depth of investigation or the AEM data might be affected by 3D effects at the bottom of the narrow structure (e.g., Goldman *et al*. 1994).

Discrepancies are also observed between AEM results compared to the borehole information and the shallow inter-till seismic reflector illustrated in Fig. 4b. Although there is good agreement in depth between the AEM result and the shallow seismic reflector, the borehole geophysical logs indicate a resistive surface layer (Crow *et al*. 2012). If we apply a starting inversion model to be resistive to a depth of 10 m, we recover a resistive surface layer, but at the cost of high misfit at early times (even though the first two data gates have already been removed). These observations suggest the presence of additional inaccuracies in the early times, possibly due to transmitter-receiver timing issues or leaking currents after the nominal end of waveform (e.g., Macnae and Baron-Hay 2010).

VTEM

Previous investigations of the Spiritwood VTEM data resulted in a VTEM model that is consistent with existing seismic, ERT and borehole data. The VTEM data were calibrated to the supporting information via a small time-shift in the VTEM data gates relative to ramp-off (Sapia *et al.* 2014). The source of the time shift was attributed to timing or turn-off errors, but the calibration procedure is independent of the source of noise. The resulting VTEM model exhibits detailed delineation of the very near surface and other resistive anomalies associated with the valley fill (Fig. 5a).

AeroTEM calibration procedure

The calibration procedure developed for VTEM data was applied to the AeroTEM data. However, matching the AeroTEM model to the ERT model proved to be difficult due to the difference in resolution and the low bandwidth of the AeroTEM data as compared to the VTEM data. Exploratory time shifts applied to the AeroTEM data did not result in appreciable changes to the model in the near-surface or at the scale of features observed in the ERT model. Furthermore, the VTEM data were flown parallel to the ERT profiles whereas the AeroTEM data were flown obliquely resulting in limited spatial overlap between these two datasets. The two AEM datasets are also energizing similar volumes of subsurface. It was therefore decided to use the VTEM model to calibrate the AeroTEM data with a data-space calibration procedure.

The VTEM model is considered as a reference model to forward model the AeroTEM response only at coincident locations (within 20 m). The overlap between the flight lines of the two

surveys is about one coincident sounding each 400 m along the VTEM flight (Fig. 1, inset). Each synthetic AeroTEM sounding (over the VTEM reference model) is compared to the corresponding observed AeroTEM sounding. Discrepancies between the VTEM and AeroTEM datasets show up as a mismatch between the synthetic and observed AeroTEM responses, mainly at early times. Guided by previous experience (Sapia *et al*. 2014) we iteratively apply small shifts to the AeroTEM time gates until we achieve a better early-time fit between the measured and synthetic AeroTEM data (not shown here). By doing this, we obtain an average shift of –20 μs to be applied to all AeroTEM time gates. Note that the first and second AeroTEM data gates are not included in this calibration and after calibration, the first useable gate is approximately 100 μs after turn-off.

We compare the model derived from calibrated AeroTEM data to the VTEM reference model (Fig. 5) and to that derived from uncalibrated data (Fig. 6). The time shift results in a reduced misfit between observed and predicted data (not shown here) and increased resistivity of the model surface. However, striping between flight lines persists in some locations and additional refinements are required to eliminate offsets between line-to-line soundings which may persist due to drift and levelling. At this point, we could revisit our calibration and include an amplitude shift of the AeroTEM data. Alternatively, we can employ an amplitude shift factor within the SCI framework to mitigate line-to-line variation in signal amplitude (Podgorski *et al*. 2013, Brodie and Sambridge 2006). The line-to-line shift factor allows the inversion to vary the sounding amplitude by as much as 50% between adjacent soundings across flight lines. Moreover, we allow variation of 1% between sounding amplitude-salong flight lines to account for steady drift (Podgorski *et al*. 2013). The result shown in Fig. 7 is almost completely free of striping with increased lateral continuity of the resistive surface. Figure 8 shows the inversion residuals and recovered amplitude shift factors. As expected, the shift factors are spatially correlated with a strong alignment along flight lines. As per the constraints, recovered shift factors exhibit large differences across flight lines (from 15% down-shifted, to almost 30% up-shifted) and only limited variability along flight lines.

Joint Inversion

Joint inversion results for both the VTEM and AeroTEM data after calibration are presented in Fig. 9t The distances between AeroTEM and VTEM coincident soundings range from approximately 10 m to 20 m. We designed the constraints so that any soundings falling within 20 m were tightly constrained. Beyond this reference distance, the effect of the constraints decreases with a partially dependent covariance that is scaled according to distance. As separate inversions, the different datasets produce two different smooth models that are correlated, in general, but at different levels of detail, especially at the very near surface (Fig. 5). The AeroTEM data consist of 17 variable width off-time measurement gates with the first usable calibrated gate time of 100 μs after ramp-off and the last gate at

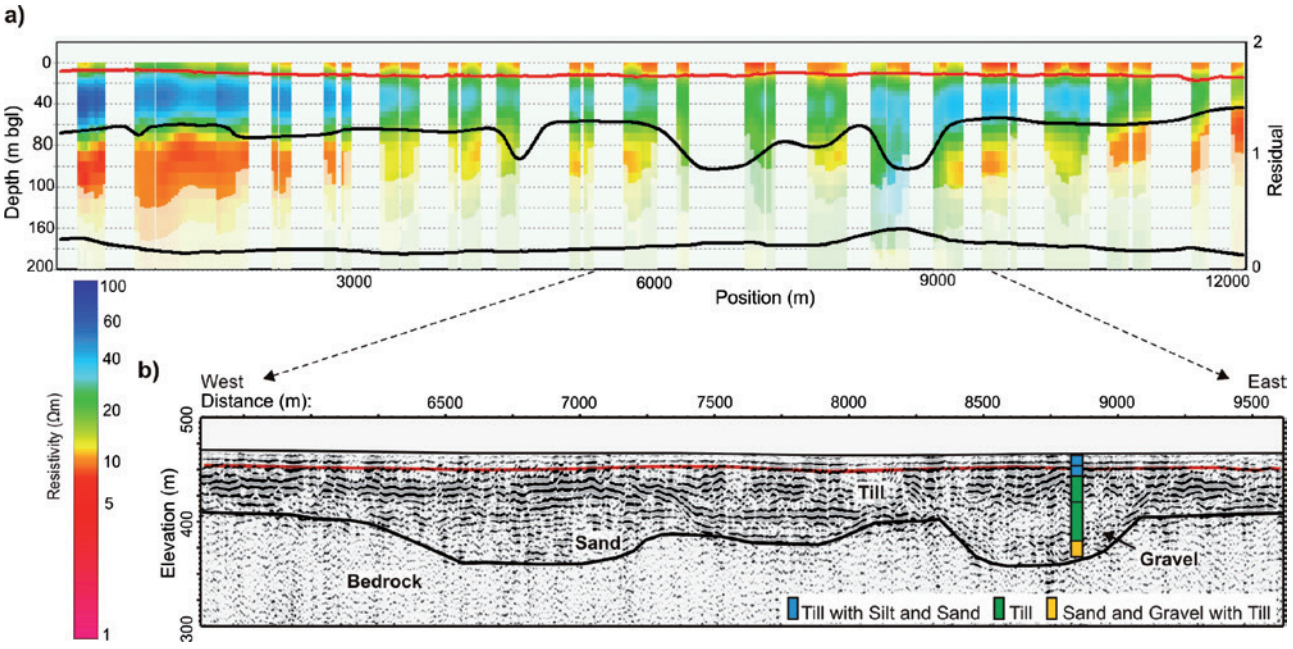

FIGURE 4

Comparison of AeroTEM III results to seismic and borehole information. a) AeroTEM III inversion results along the seismic section located in Fig. 1. Solid red line is the shallow inter-till reflection surface. Upper solid black line is the bedrock reflection surface and lower solid black line is the data misfit. Only soundings free of cultural interference and within 250 m of the seismic section are included. b) Seismic reflection section along a portion of the AEM profile showing interpretations of the main seismic reflection surfaces and a simplified description of borehole GSC-SW-07.

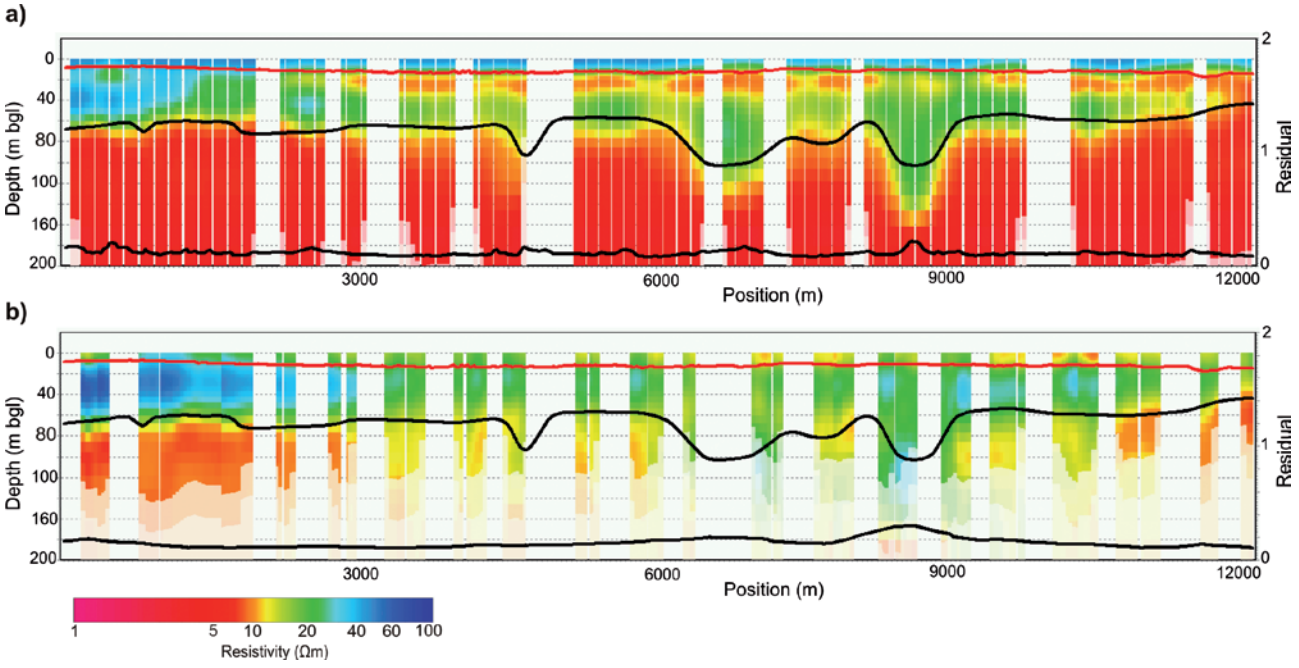

FIGURE 5

Comparison of VTEM and AeroTEM results along seismic section located in Fig. 1. a) VTEM reference model. b) AeroTEM III inversion results incorporating a –20 μs shift of all time gates. Solid red line is the shallow inter-till reflection surface. Upper solid black line is the bedrock reflection surface and lower solid black line is the data misfit.

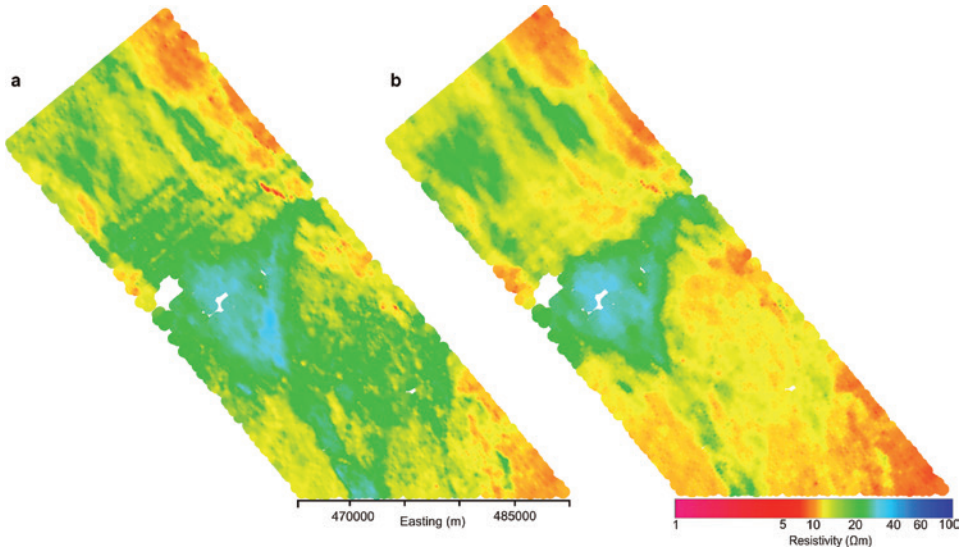

FIGURE 6

Effect of calibration on the AeroTEM III inversion result from 0–10 m depth. a) Calibration with a –20 μs shift. b) Uncalibrated (as in Fig. 3a).

approximately 3 ms. In contrast, the VTEM data consist of 44 measurement gates with the first usable calibrated gate time of 10 μs after ramp-off and the last gate at approximately 9 ms. We expect that the VTEM data will be more sensitive to the near-surface and this is evident if we consider the conductive layer at about 15 m depth (10 m thick) which is not recovered in inversion of the AeroTEM data alone (Fig. 9 vs. Fig. 5b). Nevertheless, addition of the AeroTEM data in the joint inversion results in thinning of this layer and a reduction in the resistivity of the surface layer which demonstrates that the AeroTEM data do convey some information to the joint model even in the near-surface.

The VTEM data will also better detect slow decays or late-time responses associated with deep conductive bedrock. After joint inversion, the two inset valleys appear as resistive features with clear bottoms extending up to a depth of 140 m. This result contrasts with the available seismic data which suggest a depth of about 100–110 m to the bottom of the buried valleys. Again,

we do not exclude that such narrow structures like those found at Spiritwood Valley can distort the eddy currents at depth and give rise to potential 3D effects (Goldman *et al*. 1994). The map of the data residual in Fig. 9b shows values that are largely below unity indicating how the predicted data, for both AeroTEM and VTEM soundings, fit the observed data within the noise level. Although the data residual is generally low, we observe a sharp increase of the misfit anytime an AeroTEM sounding is jointly inverted with the closest VTEM sounding. In particular, we note a significant increase in misfit where the AeroTEM data are unable to resolve the bottom of the buried valleys, but that the valley bottoms are not inconsistent with the AeroTEM data. Hence, the increases in data misfit likely reflect discrepancies due to both different near surface resolution capabilities and bedrock depth detection between the two AEM datasets.

In addition to considering the calibrated AeroTEM and VTEM data, we also performed a joint inversion of the AEM datasets as provided by the contractors without any processing for early-time bias, cultural noise, late-time noise or calibration. Figure 10 shows a profile of the inversion results along with the associated data residual. The overburden structure reverts to conductor-over-resistor as opposed to resistor-over-conductor-over-resistor

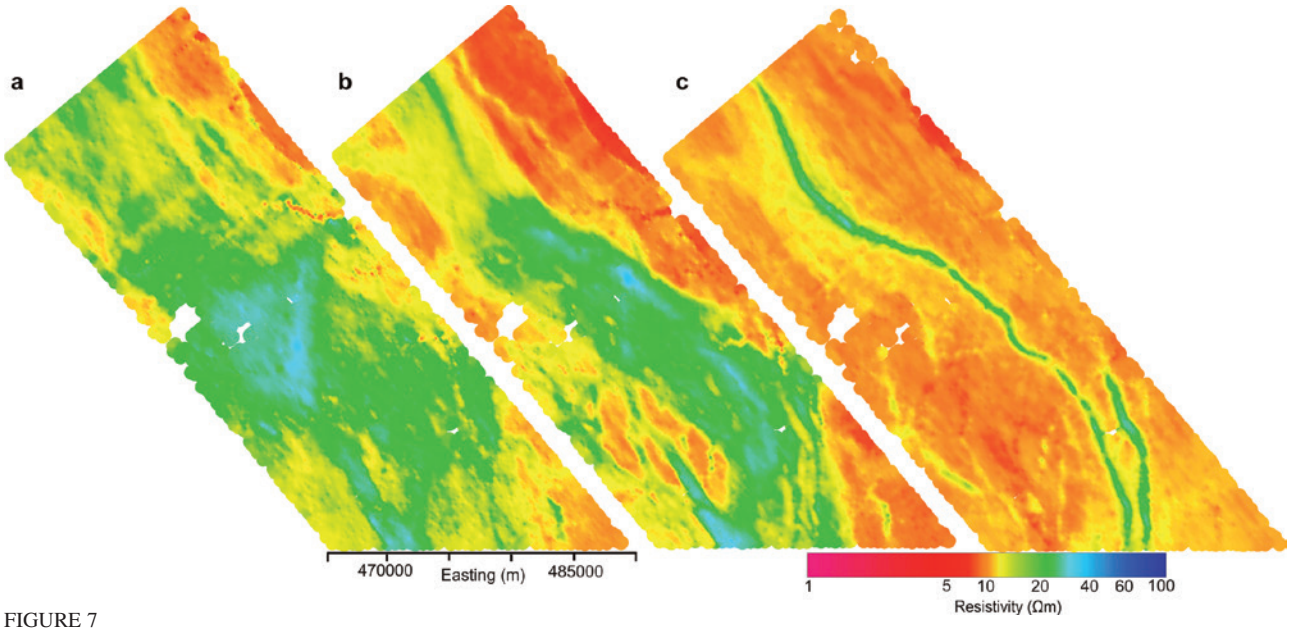

FIGURE 7

Amplitude-corrected calibrated AeroTEM III inversion results obtained with an amplitude shift factor of 1.5 across flight lines. The recovered resistivity model is shown as maps of resistivity averaged over different depth intervals: a) 0–10 m, b) 50–60 m and c) 110–120 m.

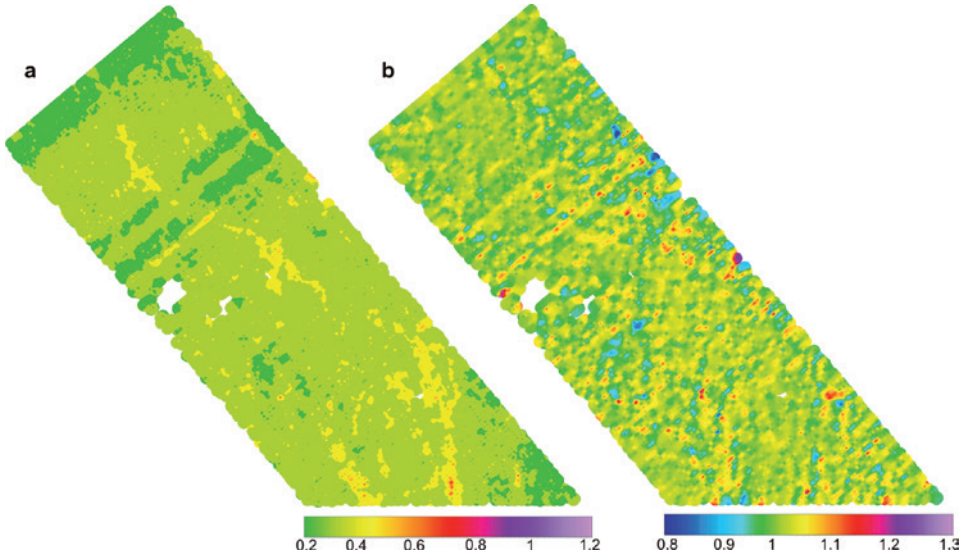

FIGURE 8

a) AeroTEM III data residual (mean squared difference, weighed against noise level for each gate). Data residual remains below 0.6 throughout the survey area. The influence of the inset valley on the residual may be a result of 3D effects associated with the narrow and deep geometry. b) Inverted amplitude shift factor varies between 0.8 and 1.3 along adjacent flight line; lineations clearly parallel the flight lines.

(Fig. 9a). The conductive layer near 15 m depth disappears completely. Also, the data residual is mostly above unity which means that we're not fitting observed data within noise level (Fig. 10b).

Resistivity maps are extracted from the unprocessed and the processed/calibrated joint inversions on the left and right of Fig. 11, respectively. In general, we observe that the model changes drastically where the two datasets overlap. This is evident for the unprocessed data at all depths, while it is signifi-

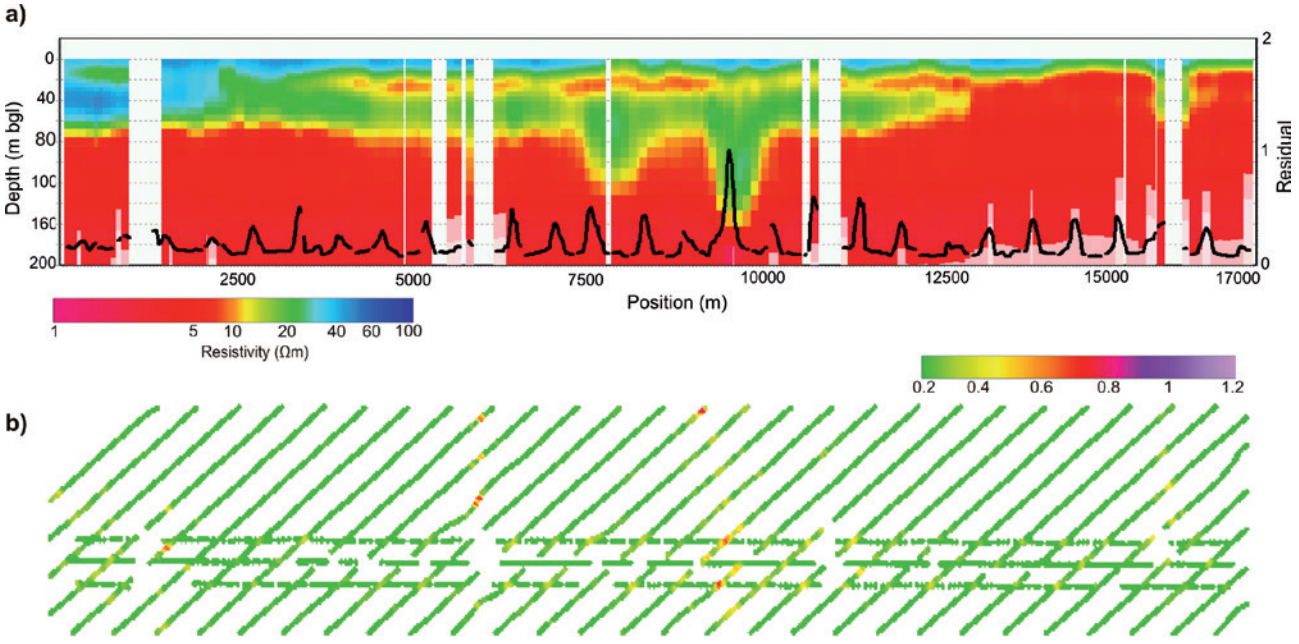

FIGURE 9

a) Joint inversion results for calibrated VTEM and AeroTEM data along the seismic section located in Fig. 1. Solid black line is the data residual. Both AeroTEM III and VTEM datasets are fully-processed and calibrated. b) Map view of the data residual.

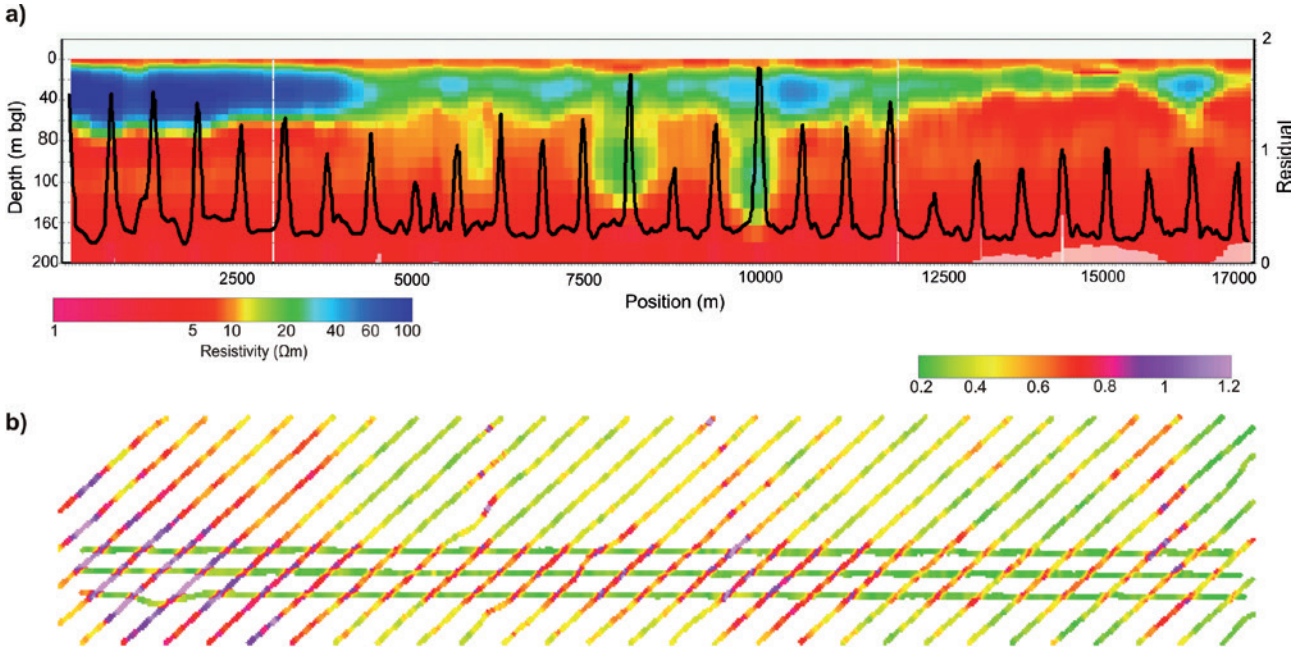

FIGURE 10

a) Joint inversion results for unprocessed and uncalibrated VTEM and AeroTEM data along the seismic section located in Fig. 1. Solid black line is the data residual. b) Map view of the data residual.

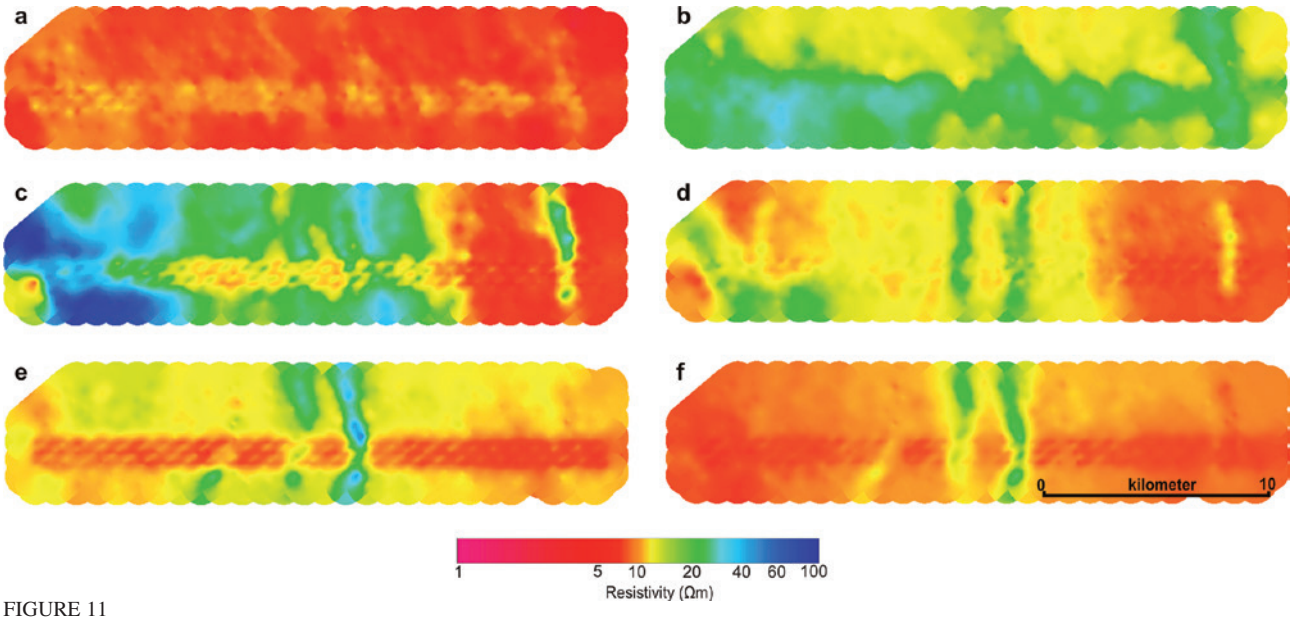

FIGURE 11
Effect of processing and calibration on joint inversion. Unprocessed and uncalibrated results at: a) 0–10 m, c) 50–60 m and e) 110–120 m depth. Fully-processed and calibrated results at: b) 0–10 m, d) 50–60 m and f) 110–120 m depth.

cantly mitigated for the calibrated joint inversion results except for the near surface. In particular, systematic striping along flight lines makes it difficult to carry out any hydrogeological interpretations of the unprocessed joint inversion result at depth (Fig. 11e vs. Fig. 11f). Furthermore, the unprocessed joint inversion result has a conductive near surface (Fig. 11a) and lacks resolution of the main resistive structures that are well resolved as inset channels in the processed/calibrated joint inversion at intermediate depths (Fig. 11c vs. Fig.11d). In addition to the main channels, other secondary valley-like-features in the western portion of the overlap areas are unclear in unprocessed joint inversion results.

DISCUSSION

Airborne geophysics can be used to significantly improve geological and hydrogeological knowledge on a regional scale (Møller *et al*. 2009, Auken *et al*. 2008, Jørgensen *et al*. 2009, Oldenborger *et al*. 2013). Many of the issues described in this paper could be relevant to other AEM datasets collected over the world. The suggested approach can be applied to any airborne EM dataset for which some reference model can be established. In our case, the VTEM model provides a reference for the AeroTEM calibration.

Our calibration procedure results in a time shift of –20 μs for AeroTEM III data collected over the Spiritwood buried valley, and the calibration results in good correlation with the reference model and ancillary information (Fig. 12). This is a pragmatic approach in that we do not attempt to identify the source of timing error, but rather, consider recovery of a consistent and acceptable model as justification of the procedure. It is important to note that the reference model should be of high quality and that any errors or uncertainty in the reference model will be propagated to the calibration and the recovered models.

With respect to the calibration time shift, there are several issues in airborne TEM data collection that can potentially affect the correct location of data gates with respect to the transmitter waveform, especially in the early stages. These include transmitter-receiver synchronization, imperfect bucking of large primary fields or parasitic capacitance (Macnae and Baron-Hay 2010). There can also be a degree of subjectivity in choosing to use ramp-off as a time reference for the receiver data gates. As a result, there can be a significant amount of current still flowing in the transmitter loop during the early off-time gates. It is unlikely that a single optimal time-shift exists for a large data set with multiple flights, although our utilization of a time shift obtained over one line of collocated data produces acceptable results survey-wide. The entire processing and calibration procedure in itself is model independent and should work in all geological domains of the survey area.

Despite calibration, the recovered resistivity maps still reveal the presence of other artefacts that appear to be flight-related. The time shift alone does not eliminate lineations observed in both the uncalibrated and calibrated inversion results. We suspect that this is a problem of signal drift and levelling across different lines and we therefore introduce an amplitude shift factor as an extra parameter in the SCI. Again our approach is pragmatic in that the source of lineations, or the nature of the recovered amplitude shift factors need not be identified. Our observations indicate amplitude variations that are spatially correlated with long-range, along-line persistence, but cross-line variability. Some of these characteristics are at least partly attributable to the inver-

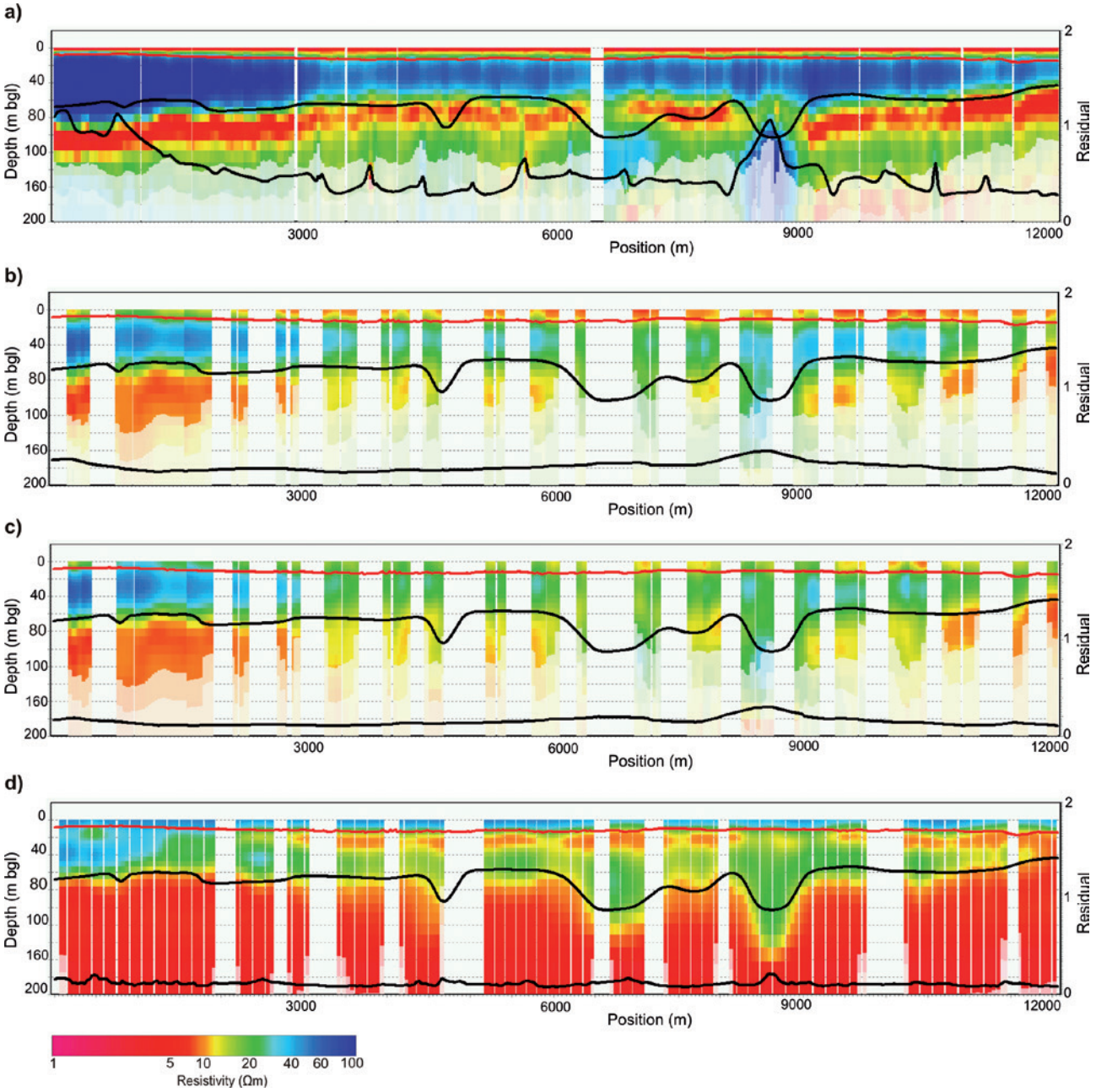

FIGURE 12

Comparison of inversion results along the seismic section located in Fig. 1. a) Unprocessed AeroTEM data. b) Fully-processed AeroTEM data. c) Fully-processed and calibrated AeroTEM data. d) VTEM reference model. Solid red line is the shallow inter-till reflection surface. Upper solid black line is the bedrock reflection surface and lower solid black line is the data misfit.

sion constraints. The recovered amplitude shift factors bear a strong resemblance in pattern and magnitude to noise associated with pendulum motion of the AEM bird observed by Davis *et al.* (2006). However, we are unable to conclusively identify pendulum effects in the AeroTEM data and the spatial characteristics of the amplitude shift factor cannot be attributed to pendulum motion alone. Other sources of noise could be aperiodic uncoupled bird motion, but AeroTEM data are not collected with enough navigational data to recover system orientation. Regardless, solving for an amplitude shift factor within the SCI can simultaneously account for multiple sources of correlated or uncorrelated noise.

CONCLUSION

Inversions of the Spiritwood AEM datasets show significant geological structures and clearly indicate a complex valley mor-

phology that can be used to significantly improve geological and hydrogeological knowledge on a regional scale. Resistivity models reveal multiple resistive valley features inside a wider valley structure. However, model reliability and resolution of the very near surface is a crucial part of groundwater mapping especially in glacial environments where multiple inter-till aquifers can occur at different depths and recharge can depend strongly on the characteristics of the entire stratigraphic sequence.

We consider the most reliable model to be one that is consistent with all available data. To this end, we developed a multi-step approach towards integration of multiple AEM surveys with different survey extents and different inherent resolving capability. The approach utilizes a combination of ancillary information in the construction of an AEM reference model and calibration of the AEM data. We suggest a protocol where a calibrated AEM dataset can be used to calibrate others. Cross-calibration of the AEM datasets produces results that are consistent with ancillary information. Joint inversion demonstrates the degree of consistency between the different AEM systems and confirms the feasibility of the cross-calibration approach, which can be useful for reconciling large volumes of existing AEM data.

ACKNOWDLEGEMENTS

The Spiritwood AeroTEM dataset is freely available from Natural Resources Canada. A. Pugin provided the interpreted seismic reflection sections. We are grateful to Geotech Ltd. for the VTEM data and the HGG group at Aarhus University for providing Aarhus Workbench and computing hardware. We thank R. Smith and J. Macnae for constructive reviews that improved the paper. In particular, J. Macnae suggested that the recovered amplitude shifts may be a manifestation of pendulum motion of the compact, low-drag AeroTEM III system.

REFERENCES

Auken E., Jørgensen F. and Sørensen K.I. 2003. Large-scale TEM investigation for groundwater. *Exploration Geophysics* **33**, 188–194. doi: 10.1071/EG03188.

Auken E., Christiansen A.V., Jacobsen L.H. and Sørensen K.I. 2008. A resolution study of buried valleys using laterally constrained inversion of TEM data. *Journal of Applied Geophysics* **65**, 10–20. doi:10.1016/j.jappgeo.2008.03.003.

Auken E., Christiansen A.V., Westergaard J.H., Kirkegaard C., Foged N. and Viezzoli A. 2009. An integrated processing scheme for high-resolution airborne electromagnetic surveys, the SkyTEM system. *Exploration Geophysics* **40**, 184–192. doi:10.1071/EG08128.

Brodie R.S. and Sambridge M. 2006. A holistic approach to inversion of frequency domain airborne EM data. *Geophysics* **71**, 301–312. doi: 10.1190/1.2356112.

Christiansen A.V., Auken E. and Viezzoli A. 2011. Quantification of modeling errors in airborne TEM caused by inaccurate system description. *Geophysics* **76**, 43–52. doi: 10.1190/1.3511354.

Christiansen A.V., Auken E., Foged N. and Sørensen K.I. 2007. Mutually and laterally constrained inversion of CVES and TEM data: a case study. *Near Surface Geophysics* **5**, 115–123. doi: 10.3997/1873-0604.2006023.

Crow H.L., Knight R.D., Medioli B.E., Hinton M.J., Plourde A., Pugin A.J.-M. *et al*. 2012. Geological, hydrogeological, geophysical, and geochemistry data from a cored borehole in the Spiritwood buried valley, southwest Manitoba. Geological Survey of Canada, Open File 7079, doi:10.495/291486.

Danielsen J.E., Auken E., Jorgensen F., Sondergaard V. and Sorensen K.I. 2003. The application of the transient electromagnetic method in hydrogeophysical surveys. *Journal of Applied Geophysics* **53**, 181–198.

Davis A., Macnae J. and Robb T. 2006. Pendulum motion in airborne HEM systems. *Exploration Geophysics* **37**, 355–362. doi: 10.1071/EG06355.

Goldman M., Tabarovsky L. and Rabinovich M. 1994. On the influence of 3-D structures in the interpretation of transient electromagnetic sounding data. *Geophysics* **59**, 889–901. doi: 10.1190/1.1443648.

Huang H. and Rudd J. 2008. Conductivity-depth imaging of helicopter-borne TEM data based on a pseudolayer half-space model. *Geophysics* **73**, 115–120. doi: 10.1190/1.2904984.

Jørgensen F. and Sandersen P.B.E. 2006. Buried and open tunnel valleys in Denmark - erosion beneath multiple ice sheets. *Quaternary Science Reviews* **25**, 1339–1363. doi:10.1016/j.quascirev.2005.11.006.

Jørgensen F. and Sandersen P.B.E. 2009. Buried Valley mapping in Denmark: evaluating mapping method constraints and the importance of data density. *Zeitschrift der Deutschen Gesellschaft für Geowissenschaften* **160**, 211–223. doi: 10.1127/1860-1804/2009/0160-0211.

Jørgensen F., Scheer W., Thomsen S., Sonnenborg T.O., Hinsby K., Wiederhold H. *et al*. 2012. Transboundary geophysical mapping of geological elements and salinity distribution critical for the assessment of future sea water intrusion in response to sea level rise. *Hydrology and Earth System Sciences* **16**, 1845–1862. doi:10.5194/hess-16-1845-2012.

Legault J.M., Prikhodko A., Dodds D.J., Macnae J.C. and Oldenborger, G.A. 2012. Results of recent VTEM helicopter system development testing over the Spiritwood Valley aquifer, Manitoba. *25th SAGEEP 2012, Symposium on the Application of Geophysics to Engineering and Environmental Problems*, Tucson, Arizona, USA, Expanded Abstracts.

Lines L.R., Schultz A.K. and Treitel S. 1988. Cooperative inversion of geophysical data. *Geophysics* **53**, 8–20. doi: 10.1190/1.1442403

Macnae J.C., Smith R., Polzer B.D., Lamontagne Y. and Klinkert P.S. 1991. Conductivity-depth imaging of airborne electromagnetic step response data. *Geophysics* **56**, 102–114. doi: 10.1190/1.1442945.

Macnae J.C. and Baron-Hay S. 2010. Reprocessing strategy to obtain quantitative early-time data from historic VTEM surveys. *21st International Geophysical Conference & Exhibition*, ASEG, Sydney, Australia.

Meju M.A. 1996. Joint inversion of TEM and distorted MT soundings: Some effective practical considerations. *Geophysics* **61**, 56–65. doi: 10.1190/1.1443956.

Møller I., Søndergaard V.H., Jørgensen F., Auken E. and Christiansen A.V. 2009. Integrated management and utilization of hydrogeophysical data on a national scale. *Near Surface Geophysics* **7**, 647–659. doi: 10.3997/1873-0604.2009031

Oldenborger G.A., Pugin A.J.-M. and Pullan S.E. 2013. Airborne time-domain electromagnetics, electrical resistivity and seismic reflection for regional three-dimensional mapping and characterization of the Spiritwood Valley Aquifer, Manitoba, Canada. *Near Surface Geophysics* **11**, 63–74. doi: 10.3997/1873-0604.2012023.

Palacky G.J. and West G.F. 1991. Airborne electromagnetic methods. In: *Electromagnetic Methods in Applied Geophysics*, Vol. 2, (ed. M.N. Nabighian), pp. 811–877, SEG Investigations in Geophysics.

Podgorski J.E., Auken E., Schamper C., Christiansen A.V., Kalscheuer T. and Green A.G. 2013. Processing and inversion of commercial helicopter time-domain electromagnetic data for environmental assessments and geologic and hydrologic mapping. *Geophysics* **78**, 149–159. doi:10.1190/GEO2012-0452.1.

Pugin A.J.-M., Pullan S.E., Hunter J.A. and Oldenborger G.A. 2009a. Hydrogeological prospecting using P and S-wave landstreamer seismic reflection methods. *Near Surface Geophysics* **7**, 315–327. doi: 10.3997/1873-0604.2009033.

Pugin A.J.-M., Oldenborger G.A., Cummings D.I., Russell H.A.J. and Sharpe D.R. 2014. Architecture of buried valleys in glaciated Canadian Prairie regions based on high resolution geophysical data. *Quaternary Science Reviews* **86**, 13–23.

Pugin A.J.-M., Oldenborger G.A. and Pullan S. 2011. Buried Valley imaging using 3-C seismic reflection, electrical resistivity and AEM surveys. *SAGEEP 2011*, Charleston, South Carolina, USA. Extended Abstract.

Raiche A.P., Jupp D.L.B., Rutter H. and Vozoff K. 1985. The joint use of coincident loop transient electromagnetic and Schlumberger sounding to resolve layered structures. *Geophysics* **50**, 1618–1627. doi: 10.1190/1.1441851

Rainsford D. 2013. Personal Communication. Ontario Geological Survey, Ministry of Northern Development and Mines.

Santos F.A.M. and El-Kaliouby H.M. 2010. Comparative study of local versus global methods for 1D joint inversion of direct current resistivity and time-domain electromagnetic data. *Near Surface Geophysics* 8, 135–143. doi:10.3997/1873-0604.2009056.

Sapia V., Oldenborger G.A., Viezzoli A. and Marchetti M. 2014. Incorporating ancillary data into the inversion of airborne time-domain electromagnetic data for hydrogeological applications. *Journal of Applied Geophysics* **104**, 35–43. doi: 10.1016/j.jappgeo.2014.02.009.

Schmutz M., Albouy Y., Guérin R., Maquaire O., Vassal J., Schott J.J. *et al*. 2000. Joint electrical and time domain electromagnetism (TDEM) data inversion applied to the Super Sauze earthflow (France). *Surveys in Geophysics* **21**, 371–390. doi: 10.1023/A:1006741024983.

Siemon B., Christiansen A.V. and Auken E. 2009. A review of helicopter-borne electromagnetic methods for groundwater exploration. *Near Surface Geophysics* **7**, 629–646. doi:10.3997/1873-0604.2009043

Sorensen C., Munday T. and Cahill K. 2012. Different aem systems = different results… or should that necessarily be the case? *SAGEEP 2012*, Tucson, Arizona, USA.

Steuer A., Siemon B. and Auken E. 2009. A comparison of helicopter-borne electromagnetic in frequency- and time-domain at the Cuxhaven valley in Northern Germany. *Journal of Applied Geophysics* **67**, 194–205, doi: 10.1016/j.jappgeo.2007.07.001.

Viezzoli A., Christiansen A.V., Auken E. and Sørensen K. 2008. Quasi-3D modeling of airborne TEM data by spatially constrained inversion. *Geophysics* **73**, 105–113. doi: 10.1190/1.2895521.

Vozoff K. and Jupp D.L.B. 1975. Joint inversion of geophysical data. *Geophysical Journal of the Royal Astronomical Society* **42**, 977–991. doi: 10.1111/j.1365-246X.1975.tb06462.x.

Winter T.C., Benson R.D., Engberg R.A., Wiche G.J., Emerson D.G., Crosby O.A. and Miller J.E. 1984. Synopsis of ground-water and surface-water resources of North Dakota. United States Geological Survey, Open File Report 84-732.

Wisén R. and Christiansen A.V. 2005. Laterally and mutually constrained inversion of surface wave seismic data and resistivity data. *Journal of Environmental & Engineering Geophysics* **10**, 251–262. doi: 10.2113/JEEG10.3.251.